Journal of Hazardous Materials 183 (2010) 324–333

Contents lists available at ScienceDirect

Journal of Hazardous Materials

journal homepage: www.elsevier.com/locate/jhazmat

RETRACTED

Frictional properties of single crystals HMX, RDX and PETN explosives

Y.Q. Wu*, F.L. Huang

State Key Laboratory of Explosion Science and Technology, Beijing Institute of Technology, 100081, Beijing, PR China

ARTICLE INFO

Article history:
Received 6 May 2010
Received in revised form 6 July 2010
Accepted 8 July 2010
Available online 15 July 2010

Keywords:
Secondary explosive crystals
Coefficient of friction
Environmental scanning electron microscopy

ABSTRACT

The frictional properties of single crystals of cyclotetramethylene tetranitramine (HMX), cyclotrimethylene trinitramine (RDX) and pentaerythritol tetranitrate (PETN) secondary explosives are examined using a sensitive friction machine. The explosive crystals used for the measurements are at least 3.5 mm wide. The friction coefficients between crystals of the same explosive (i.e., HMX on HMX, etc.), crystals of different explosives (i.e., HMX on RDX, etc.), and each explosive and a well-polished gauge steel surface are determined. The frictional surfaces are [illegible] studied under an environmental scanning electron microscope (ESEM) to analyze surface microstructural changes under increasing loading forces. The friction coefficients vary considerably with increasing normal loading forces and are particularly sensitive to slider shapes, crystal roughness and the mechanical properties of both the slider and the sample. With increasing loading forces, most friction experiments show surface damage, consisting of grooves, debris, and nano-particles, on both the slider and sample. In some cases, a strong evidence of a localized molten state is found in the central region of the friction track. Possible mechanisms that affect the friction coefficient are discussed based on microscopic observations.

1. Introduction

Among all the stimuli that may trigger the ignition and explosion of crystals, friction remains as the most universal, the most difficult to eliminate, and the least understood [1,2]. Frictional rubbing can occur between explosive crystals and a containing wall [3], between individual crystals, and between crystals and inert grits [4–6]. Friction between two surfaces, grit particles, or material grains has been studied [7,8]. Evidence based on high-speed photographic sequences of pentaerythritol tetranitrate (PETN) and cyclotetramethylene tetranitramine (HMX) explosives under a drop-weight impact loading has allowed for the discussion of friction ignition mechanisms [9,10]. However, predicting of the friction sensitivity of an energetic compound is still subject to debate [11,12]. Friction coefficient is difficult to predict because it depends on the amount of lubrication and [illegible]. An expression was developed for the friction coefficient of a material in terms of parameters that control frictional heating in explosive materials [13]. The effect of humidity on the sensitivity of cyclotrimethylene trinitramine (RDX) to initiation by friction has been studied at different temperatures. It is unclear if the effect is due to increased lubricity or water filling the micro-cracks in the RDX [14].

Determining friction sensitivity is important for recently synthesized explosive [15–18], as well as for energetic crystals, including HMX, RDX and PETN, which are extensively used in military and industrial applications because of their high energy performance, good stability, and low cost. Nitromine explosives, such as RDX and HMX are so sensitive to friction stimuli such that, for many applications, pre-treatment to decrease friction sensitivity may be beneficial [19]. Recently, research has been aimed at developing new materials with decreased friction sensitivity, and with sufficient energy densities to support combustion. These are the paths for future applications [20].

A small-scale experimental facility has been designed to investigate interfacial dynamics at high sliding speeds to obtain kinetic friction coefficients of metal materials [21]. However, data for single crystal explosives are rare. The dynamic coefficient of friction of the plastic bonded explosive (PBX) LX-04 was also measured on stainless steel, aluminum, Teflon and on the explosive itself as a function of temperature (ambient temperature to 135 °C) at a rotational speed of 0.225 rad s^{-1} [22]. Analysis indicates that the friction between the surfaces of closed cracks could result in a linear increase in compressive strength with an increase in hydrostatic pressure, and a friction coefficient could be obtained from the linear slope and the measured angle of the failure plane [23]. The stress states for which all cracks are friction-locked increase with the fiction coefficient. Some of these coefficients are provided in Refs. [24,25]. Dienes et al. used different values for the static coefficient of friction (0.8) and the dynamic coefficient of friction (0.2) for PBX explosives [26]. Friction conditions could alter the results of both drop-weight and Steven tests. Consequently, these tests could not be modeled accurately.

* Corresponding author. Tel.: +86 10 68918019; fax: +86 10 68461702.
E-mail address: wuyqing@bit.edu.cn (Y.Q. Wu).

0304-3894/$ – see front matter
doi:10.1016/j.jhazmat.2010.07.027

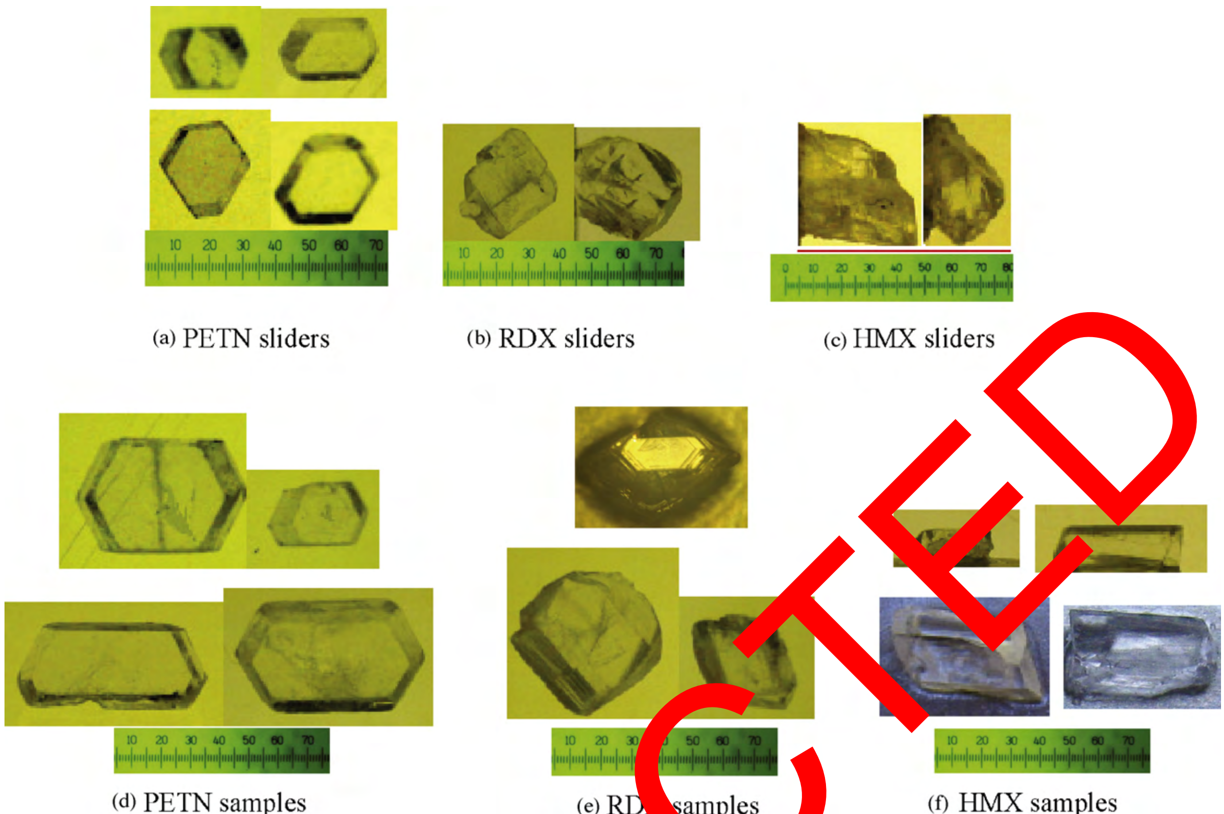

Fig. 1. As-received PETN, RDX, and HMX single crystals used as sliders and samples.

Peterson et al. suggested that some types of high explosives are relatively insensitive to pure impact and pure friction but are relatively sensitive to stimuli involving a combination of impact and friction [27]. Dickson et al. calculated the coefficient of friction for a PBX9501 sample and several grains of sand at a sliding speed of approximately 14 m s^{-1} [28].

Amuzu et al. carried out some friction experiments, involving explosive single crystal on single crystal, single crystal on glass, and a thin film of explosive material between smooth and rigid substrates [29]. However, they did not provide additional information about the material's surface characteristics. As such, their results did not completely agree with the data obtained from the present work, especially in terms of the effects of the shapes and surface characteristics of explosive crystals.

This study examines the properties of explosive crystals or composite explosives composed of HMX, PETN, RDX, which may be ignited by friction heating, especially in the low-strength impact system. Information on the coefficients of friction is important to estimating the interface temperature increase caused by friction. It is very difficult to measure directly the temperature at the interface between the different explosive crystal surfaces inside explosive materials. A thorough knowledge of the frictional properties of these explosive crystals will help in more accurately estimating the ignition stage, the initial event for deflagration, and detonation.

Frictional data for different explosive crystals are provided in Section 3. Tracks and microstructural characteristics of different sliders with different samples were observed under an optical microscope and an environment scanning electronic microscope (ESEM). The relationship between the coefficients of friction and normal loading forces, combined with surface microscopic characteristics, was analyzed to investigate different phenomena that appear during friction.

2. Experimental

Typical images of good-quality HMX, RDX, and PETN single crystals used in friction experiments are shown in Fig. 1. Some smaller crystals with sharp tips or small flat surfaces were chosen as sliders, and larger with reasonably sized crystals were selected as samples. Widths were no less than 3.5 mm to ensure full to-and-fro friction sliding. Sliders and samples were glued onto an Al stub using Evostik multi-purpose instant contact adhesive for friction force measurements. The coefficient of friction can be evaluated by various methods. The approach proposed by Andersen [13] is based on the following equation:

$$\mu = \tau \cdot \beta_e \qquad (1)$$

where β_e is the effective compressibility of the bulk material, between the loading surface and friction surface and τ is the shear stress necessary to break the contacts between the slider and the sample.

Evostik multi-purpose instant contact adhesive can form strong interface joints. The friction force F in this experiment was too low to cause relative motion between Al stub and crystal slider. Consequently, the effect of the adhesive on the shear stress τ was negligible. Due to its dimensional instability, however, the adhesive will cause β_e to drop. As a result, the adhesive lowered the resulting coefficients of friction to some extent. In order to minimize its influence, the adhesive was applied as thinly and uniformly as possible.

The friction machine used in the study was designed and fabricated at the Cavendish Laboratory (University of Cambridge, UK). The experimental setup is shown schematically in Fig. 2. The upper slider assembly was supported by a load-cell at one end of a sensitive beam balance. Loading forces from 1.5 to 28 g were applied on the Al stub using various combinations of different standard

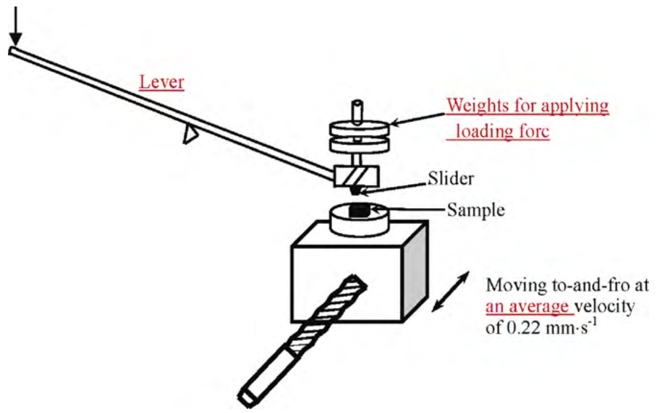

Fig. 2. A schematic graph of the friction machine presenting how to perform the friction test. The normal force is applied by various combinations of many weights. The lever needs to be adjusted horizontally prior to the experiments. The sample's assembly is driven by a motor drive set at an average velocity of 0.22 mm s^{-1}.

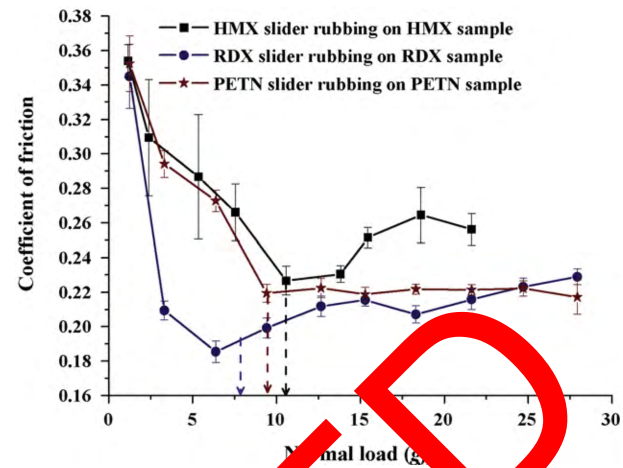

Fig. 4. Coefficients of friction for the same crystal pairs, including HMX, RDX, and PETN single crystals.

weights. Balance of the suspended beam was adjusted using a simple optical method, prior to performing the friction experiment. Samples were placed on a polymethyl methacrylate plate rigidly mounted on a goniometer, so that the horizontal orientation could be adjusted. Samples were driven by a motor drive at an average velocity of 0.22 mm s^{-1}. The measured frictional force was then outputted into a chart recorder (*Unicorder-U329*) at a recording velocity of 40 mm min^{-1}. The experiments were performed at about 20 °C. Each data point under the same loading force was repeated at least five cycles.

Calibration was performed using some known weights on a suspended by a pulley with nylon line. The calibrated lines in Fig. 3 show that the two calibration factors are 0.00224 and 0.00227 V/g at 50 and 100 mV, respectively. Frictional surfaces were also studied under an ESEM to analyze surface changes under increasing loading forces.

3. Measured results of coefficients of friction

3.1. Identical crystal pairs

Friction coefficients under different loading forces were first measured for the same crystal material pair, i.e., an HMX slider on an HMX sample, an RDX slider on an RDX sample, and a PETN slider on a PETN sample. The variations in friction coefficients with loading force, combined with the error bars for the three explosive crystal pairs, are presented in Fig. 4. At a normal loading force of 1.2 gf, the friction coefficient for all explosive crystals is around 0.35. The reason behind the similarity in friction coefficients for the three crystal pairs requires further study. Each curve is characterized by the highest coefficient of friction at the lowest loading force. In 1976, Amuzu et al. explained the dependence of the coefficient of friction on the loading force within the elastic regime based on a simple relationship of contact mechanics. As indicated by the arrow line in Fig. 4, below a certain loading force, the friction coefficients decrease monotonously with increasing applied forces for the three crystal pairs. Above this value, the friction coefficients change slightly with increasing loading forces.

Above the yielding point, the PETN crystal showed an almost constant 0.22 coefficient of friction, even with increasing loading forces. However, HMX and RDX crystals show an increase in the friction coefficients when the loading force increases to the plastic regime. HMX has the highest friction coefficient, followed by the PETN, then by RDX. Generally, in the plastic regime, the friction coefficient does not change remarkably with increasing loading force. The values for the coefficient of friction, are mostly in the range 0.20–0.25 for these three explosive crystal pairs. The origin of the plastic contact in HMX, RDX, and PETN crystals are estimated to be 10.58, 7.9 and 9.41 gf loading forces, respectively.

3.2. Dissimilar crystal pairs

As shown in Fig. 5, no elastic stage is detected in the plots of frictional coefficients for dissimilar crystal pairs. This may be due to the non-simultaneous entry of the slider and the sample into the plastic region.

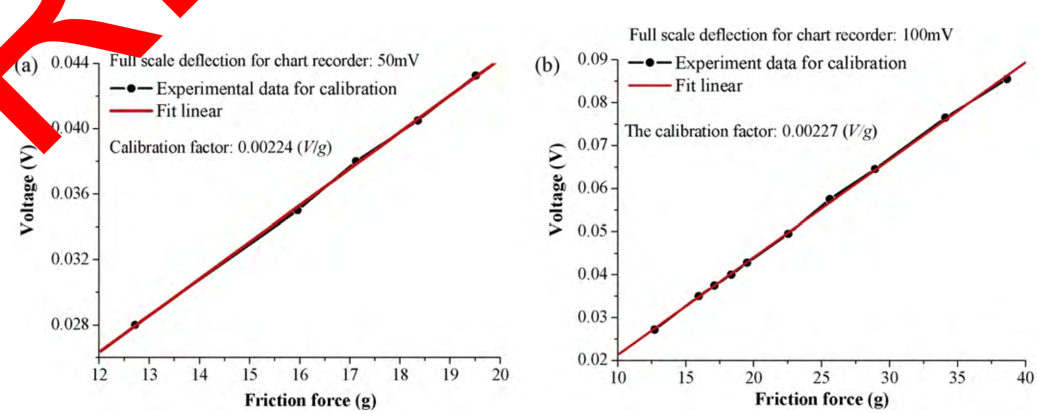

Fig. 3. Calibration curves for two full scale deflection (a) 50 mV; (b) 100 mV which were used in the friction test.

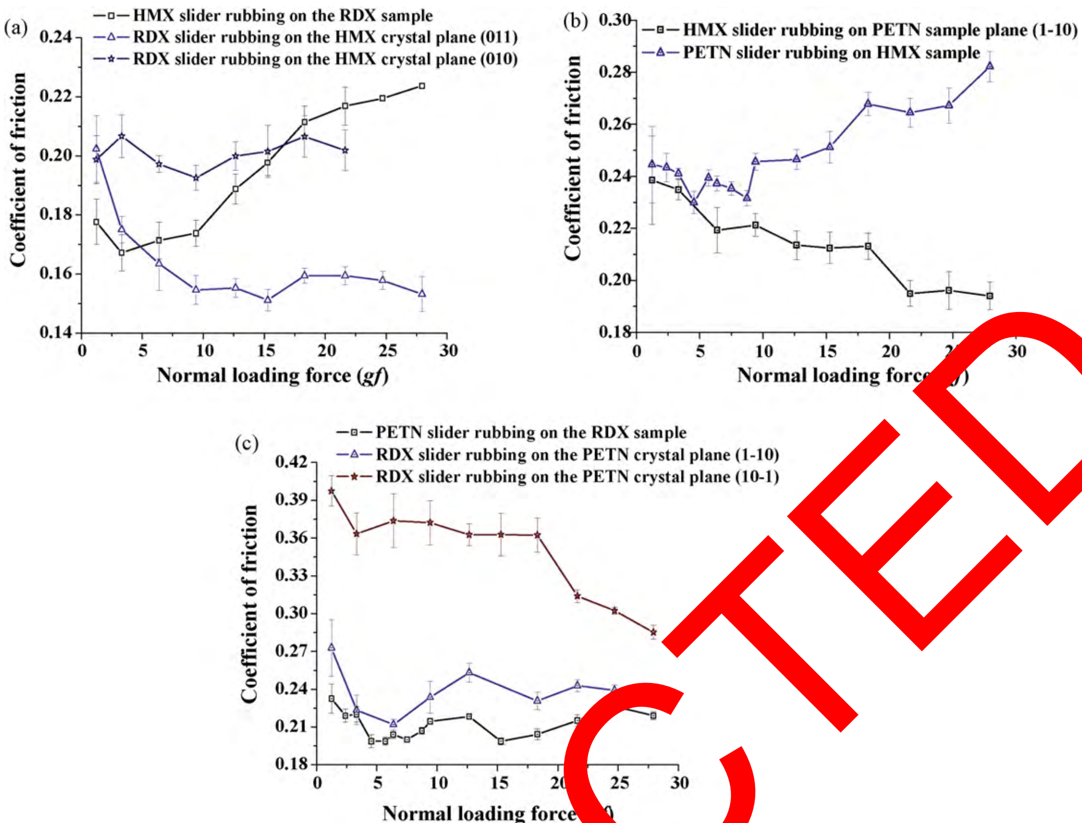

Fig. 5. Dependences of the fiction coefficients on normal loading forces for different explosive crystal material pairs including (a) HMX slider on RDX sample and RDX slider on the (0 1 1) and (0 1 0) of HMX crystal planes; (b) HMX slider on PETN sample and PETN slider on HMX sample; (c) RDX slider on the $(1\,\bar{1}\,0)$ $(1\,0\,\bar{1})$ crystal planes of PETN and PETN slider on RDX crystal.

Fig. 5(a) shows the friction coefficients between HMX and RDX crystals. The HMX crystal planes (0 1 1) and (0 1 0) were used to measure the friction coefficients with an RDX slider. Three types of plots for the friction coefficient dependence on loading force are shown in Fig. 5(a). With an HMX slider on an RDX sample, the friction coefficients increase with increasing loading forces. The friction coefficients are in the range 0.17–0.22. With an RDX slider on a (0 1 1) crystal plane of HMX, the friction coefficients decrease from 0.20 to 0.15, when loading forces are increased from 1.2 to 27.9 gf. In comparison, when an RDX slider is rubbed on the (0 1 0) crystal plane of HMX, the coefficient of friction remains relatively unchanged at around 0.2 with increasing loading forces.

Fig. 5(b) shows the coefficients of friction between the HMX and PETN crystals. With an HMX slider on a PETN sample, the friction coefficients decreased monotonically from 0.24 to 0.19 with increasing loading force. By comparison, using a PETN slider on an HMX sample the values increase from 0.24 to 0.28 when the loading force is increased from 1.2 to 27.9 gf.

Fig. 5(c) shows the coefficients of friction for an RDX slider on a PETN sample as well as a PETN slider on an RDX sample. Two different crystal planes, $(1\,0\,\bar{1})$ and $(1\,\bar{1}\,0)$, of PETN were used to measure the friction coefficients. When an RDX slider rubs on the $(1\,0\,\bar{1})$ PETN crystal plane, the friction coefficients decrease from 0.40 to 0.29, when the loading force increase from 1.2 to 27.9 gf. This pairing has the highest friction coefficients among all the reported cases. With an RDX slider on the $(1\,\bar{1}\,0)$ PETN crystal plane, the coefficients of friction are from 0.21 to 0.26. Similarly, when a PETN slider is tested on an RDX sample, the friction coefficients also change slightly which are in the range 0.20–0.23 with increasing loading forces.

Analyzing the coefficient of friction curves in Fig. 5 reveals three distinct relationships between the coefficient of friction and the normal loading force. In the first type of pairing, the coefficients of friction increase consistently with an increase in normal loading forces. In the second type, the friction coefficients decrease with increasing normal loading forces. In the last type, the friction coefficients remain almost constant with varying normal loading forces.

3.3. Crystal and steel pairs

Fig. 6 shows that the friction coefficients between the HMX/RDX/PETN crystals and steel decrease with increasing loading forces in the elastic regime, similar to that in identical crystal pairs.

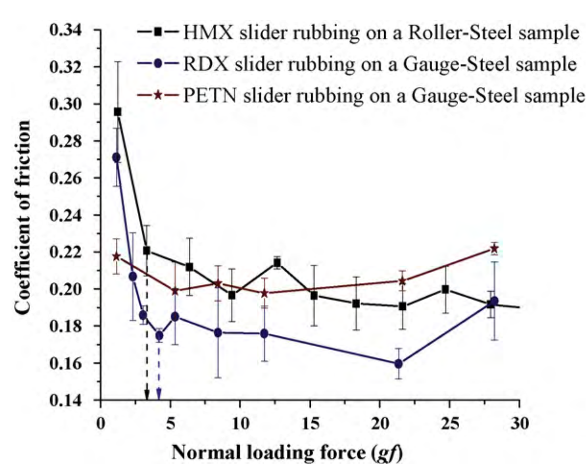

Fig. 6. Coefficients of friction for the explosive crystal material sliders rubbing on the smooth steel samples.

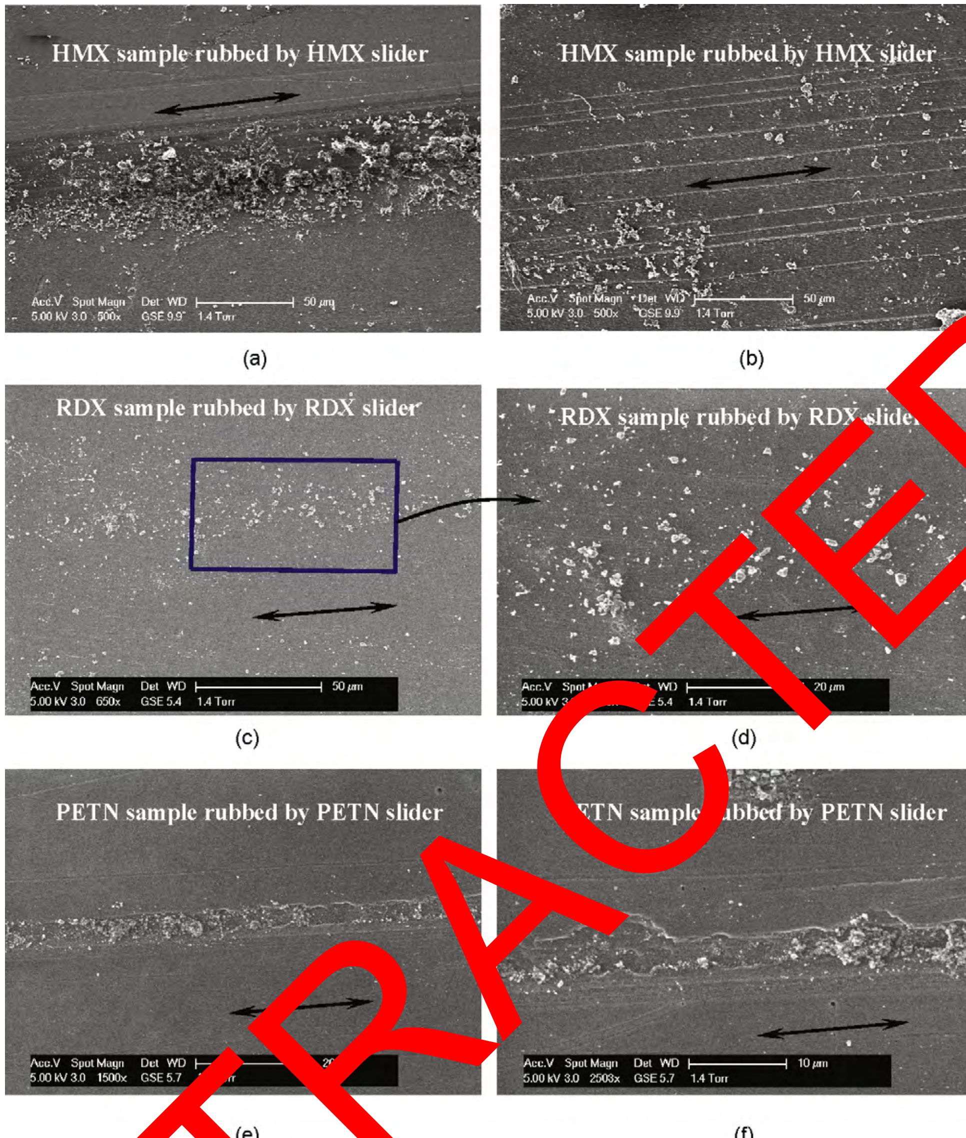

Fig. 7. Surface tracks observed by ESEM showing (a) the track produced by an HMX slider on an HMX sample at the normal load of 18.6 gf; (b) the track produced by an HMX slider on an HMX sample at the normal load of 21.6 gf; (c) tracks produced by an RDX slider on an RDX sample; (d) the track in (c) at higher magnification; (e) the track on a PETN sample produced by a PETN slider; (f) the track in (e) observed at higher magnification. The double-arrow lines indicate the friction sliding directions.

However, with a PETN slider on a steel sample, no obvious elasticity is apparent in the curve and the friction coefficients change minimally with increasing loading force. In contrast, when explosive crystals are rubbed against the [illegible] steel surface, the coefficients of friction (0.16–0.22 during the plastic stage) are lower than that of the same crystal [illegible]. The coefficients of friction for a PETN slider on steel are close to that of PETN on PETN at around 0.20–0.22.

A significant feature of the friction between explosive crystal sliders and steel samples is the transfer of explosive material from the slider to the steel surface because steel is much harder than the slider. We determined whether this transfer of material affects friction behaviors. When mass transfer occurs, the friction coefficient between explosive crystals and steel is written as follows:

$$\bar{\mu} = \chi\mu_{cr-cr} + (1-\chi)\mu_{cr-st} \quad (2)$$

where $\bar{\mu}$ is the weighted average friction coefficient, and $0 < \chi < 1$ is the weight fraction contributed by the explosive crystal slider that transferred the material. And μ_{cr-cr} and μ_{cr-st} are the true friction coefficients of the explosive crystal with steel and with similar explosive crystals, respectively. Variations in coefficients of friction with loading force, shown in Fig. 6, are similar to those for the same crystal pairs. The only difference is that the friction coefficients of explosive crystals and steel are lower than those of similar explosive crystals. These characteristics imply that μ_{cr-st} is much lower than μ_{cr-cr} because of the weighted average relationship in Eq. (1). However, the existing friction data are insufficient to calculate the weighted fraction and the true friction coefficients of explosive crystals with steel.

4. Observations of surface frictional track

4.1. Identical crystal pairs

Surface observations using an ESEM (FEI) are important in understanding complex phenomena in friction coefficient variations with loading force. Fig. 7 shows the typical tracks produced by HMX–HMX, RDX–RDX, and PETN–PETN pairs. In Fig. 7(a) and (b), the presence of many particles inside grooves at 18.6 and 21.6 gf loading forces imply that both mass transfer and ploughing occurred. Furthermore, small particles inside the track result from

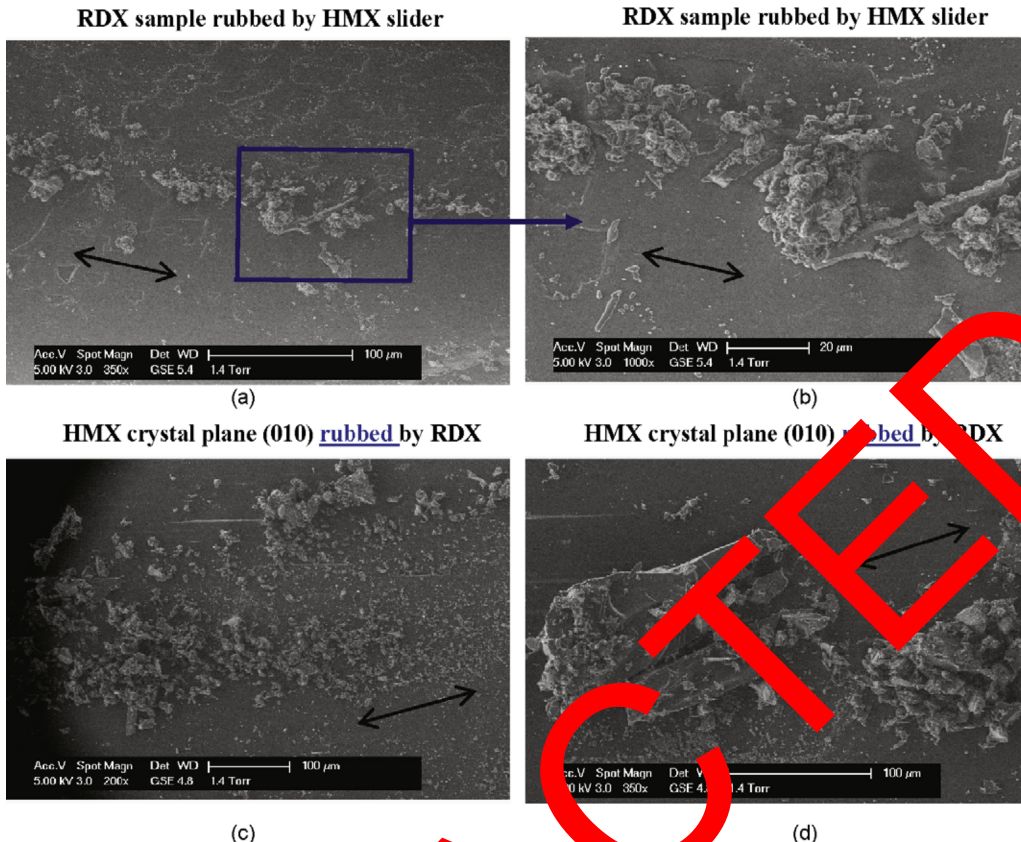

Fig. 8. Surface tracks observed by ESEM (a) on an RDX samples showing many different-sized particles distribute along the track on RDX sample rubbed by HMX slider; (b) the particles morphology observed at higher magnification; (c) different-sized particles along track on an HMX crystal plane (0 1 0) rubbed by an RDX slider; (d) some big fractured debris exist inside the track on an HMX crystal plane (0 1 0). The double-arrow lines indicate the frictional sliding direction. These photographs correspond to curves in Fig. 5(a).

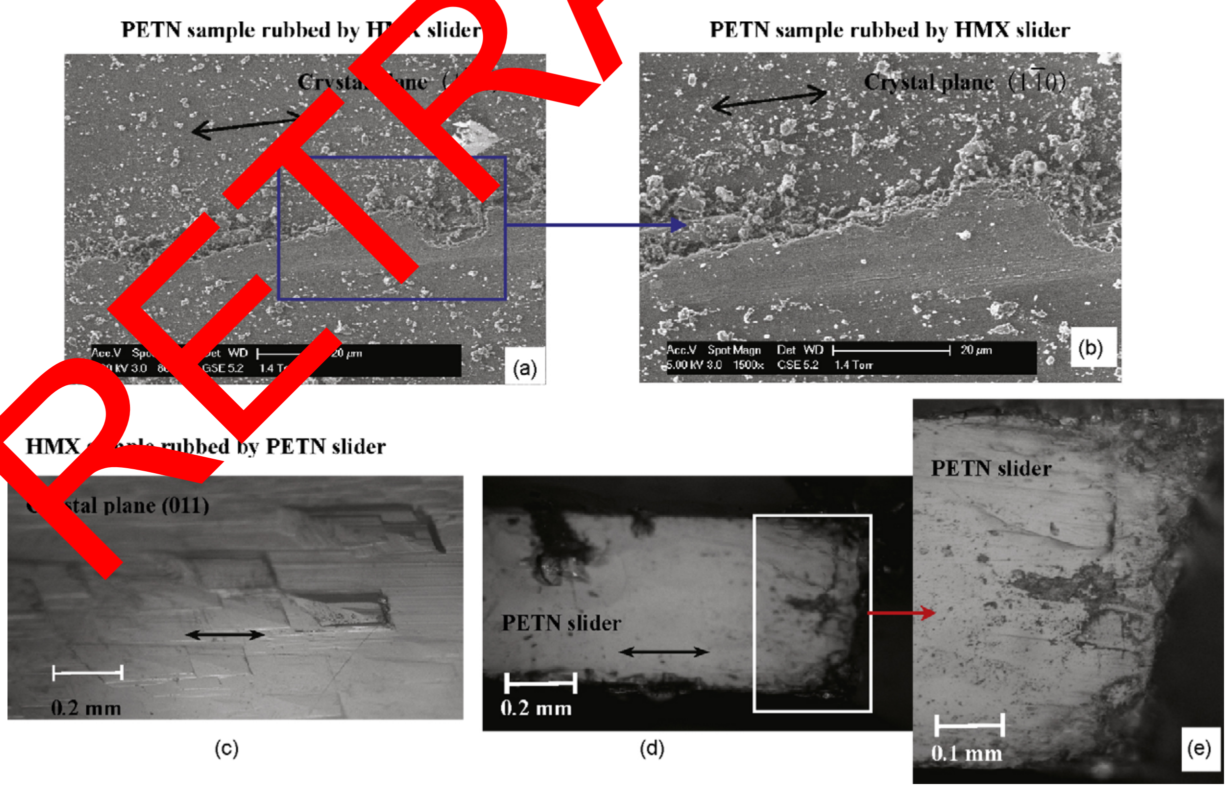

Fig. 9. Surface observations by ESEM on PETN and HMX crystals showing (a) one flat zone in the middle of the track surrounded by many particles on PETN sample surface; (b) local flatten zone at higher magnification showing the characteristics of molten substance; (c) optical photograph of HMX sample in which no tracks were observed when rubbed with a PETN slider; (d) PETN slider used for rubbing with HMX sample; (e) local abrasive damage zone at higher magnification inside the PETN slider. The double-arrow lines in the graphs indicated frictional sliding direction. These photographs correspond to the curves in Fig. 5(b).

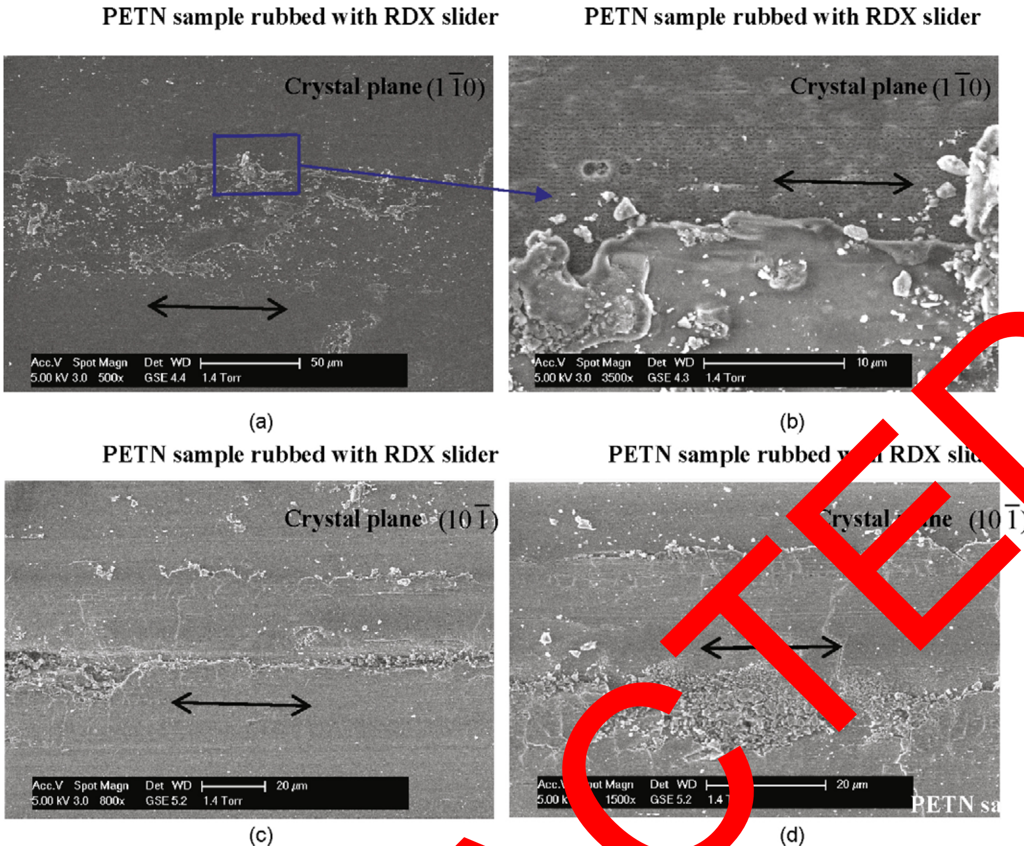

Fig. 10. Surface track observed by ESEM on PETN sample rubbed by RDX slider: (a) on PETN crystal plane $(1\bar{1}0)$; (b) local zone morphology at higher magnification; (c) on PETN crystal plane $(10\bar{1})$; (d) typical track characteristics observed at higher magnification. These photographs correspond to the curves in Fig. 5(c).

increased coefficients of friction in the plastic region. In Fig. 7(b), the tracks appear to be made of more than one line, indicating that multiple asperities operated during the frictional interaction.

Fig. 7(c) and (d) shows traces on an RDX sample rubbed by an RDX slider. Compared to HMX–HMX pairs, no deep tracks are observed and only few particles are left on the trail, making it easier to follow the sliding path. Most of the particles are less than 1.0 μm in size.

Fig. 7(e) and (f) shows the tracks made by a PETN slider rubbing on a PETN sample. The width of the track is less than 10 μm. Features of a molten substance are visible in the track. Fig. 7(f) shows a flowing trail of molten material in the middle part of the track. When the PETN slider was on a PETN sample, molten substances may act like lubricants, such that the friction coefficients remain almost constant with increasing loading forces.

4.2. Dissimilar crystal pairs

In Figs. 8–10, surface characteristics are shown for different crystal friction pairs. Fig. 8(a) and (b) shows fractured debris found inside the track of the RDX sample after rubbing with the HMX slider. Many particles of different sizes are distributed along the friction path. Because HMX is harder than RDX, contributions from ploughing may not be neglected. Such characteristics could result in a monotonic increase in friction coefficients with increasing loading forces.

Fig. 8(c) and (d) presents the track on the (0 1 0) HMX crystal plane produced by an RDX slider. This track consists of many particles and fractured debris inside the track. Compared to Fig. 8(a) and (b), the particles are expected to come from the RDX slider, instead of the HMX sample. In the latter case, the coefficients of friction decrease from 0.21 to 0.19 with increasing loading forces. As shown in previous tests, when an RDX slider rubs against an RDX crystal sample, the friction coefficient also ranges from 0.19 to 0.21. Since particles are transferred from the RDX slider to the HMX sample, the frictional interaction between the RDX slider and the (0 1 0) HMX crystal plane may likely be from the friction between the RDX slider and the RDX fragments, causing a decreasing trend in the friction coefficient given an increasing loading force.

In Fig. 9(a) and (b), surface observations of the $(1\bar{1}0)$ PETN plane rubbed by an HMX slider show a flatten zone in the middle of the track, instead of a groove due to ploughing. Such features partly result from the emergence of a molten substance, which may lead to a decreasing curve observed with the HMX slider on PETN sample. This can be explained by a decrease of the shear stress as the amount of molten substance increase.

No tracks are found on the surface of the HMX crystal after rubbing with a PETN slider. As shown in Fig. 9(c), many regular subgrain pits are present on the surface of the HMX sample. This indicates that the surface of the HMX sample is rough and has many regularly arranged subgrains. In contrast, serious abrasive damage is found on the surface of the PETN slider (Fig. 9 (d) and (e)). The PETN slider surface appears to have been ploughed by the rough HMX surface. If the asperities on the harder surface ploughed the surface of the softer material with no apparent melting, an extra force may be involved in the friction force. This may account for the increase in friction coefficients with increasing loading forces. Aside from the additional force, no other phenomenon can explain the increasing curve of the PETN slider on HMX.

Fig. 10(a) and (b) shows the track characteristics on the $(1\bar{1}0)$ PETN crystal plane after being rubbed with an RDX slider. The track width was about 50 μm. In Fig. 10(b), typical features of a flowing molten substance can be observed at the edge of the track, thus

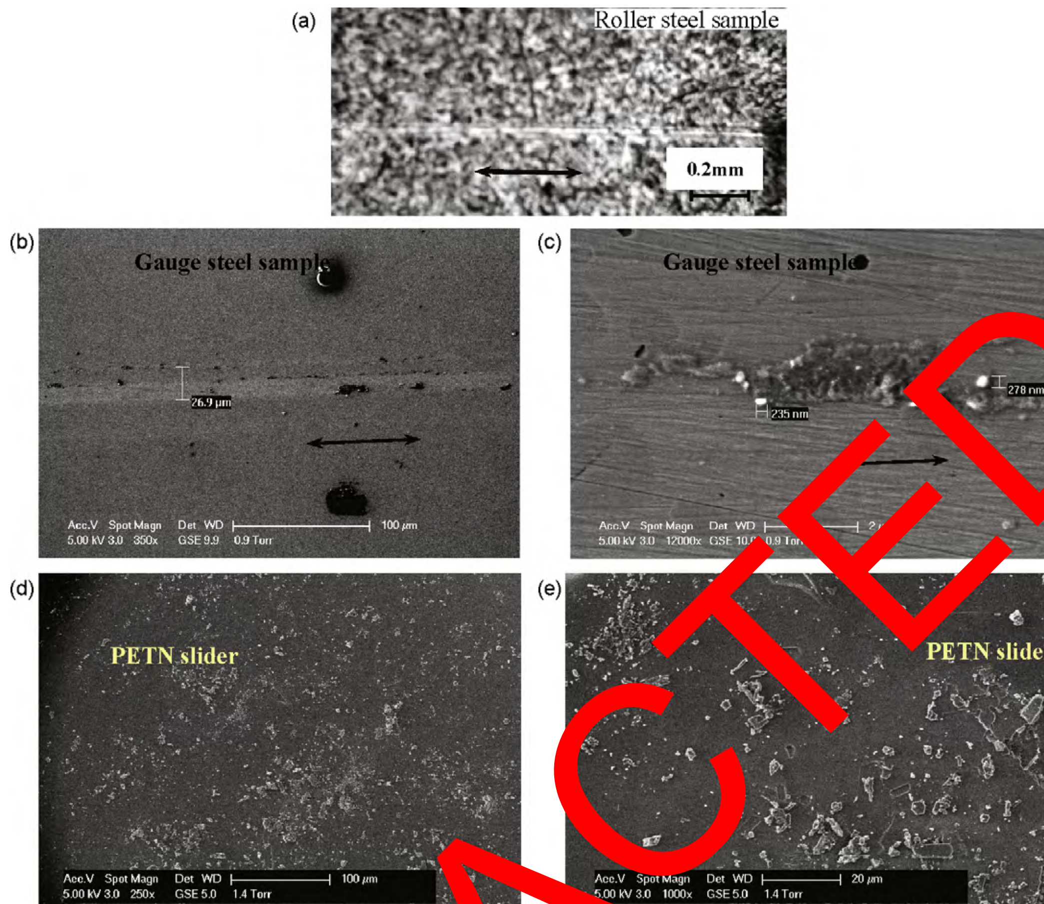

Fig. 11. Observations of the tracks showed (a) by an optical photograph on the Roller steel sample rubbed with an HMX crystal slider; (b) by ESEM on the Gauge steel sample rubbed with by an RDX crystal slider and (c) by ESEM amorphous particles at higher magnification. (d) By ESEM many broken debris inside the PETN slider but no tracks were found on the Gauge steel sample after rubbed with a PETN slider. (e) by ESEM some regular-shaped transparent fractured PETN crystals at higher magnification. The double-arrow lines indicate the frictional sliding directions.

providing conclusive evidence of the emergence of molten material from friction between the RDX slider and the PETN sample. The emergence of such a substance corresponds to a decreasing curve observed with the RDX slider rubbing on the (1 0 1̄) PETN crystal plane. The effects of the surface molten substance may directly explain the decreasing friction coefficient plot.

Fig. 10(c) and (d) shows the track on the (1 0 1̄) PETN crystal plane caused by an RDX slider. The flat zone in the middle of the track is surrounded by crushed particles. This track is comprised of the pressed molten substance mixed with the surrounding particles. Despite having the same material, Fig. 10(c) and (d) shows different characteristics from Fig. 10(a) and (b), thus demonstrating orientation-dependent frictional properties. The friction coefficients correlate well with the emergence of molten substances and particles caused by ploughing. It is apparent that molten substances play a lubricating role, whereas the particles added the frictional force. No tracks are found in the PETN slider on the RDX sample. Microscopic observations showed that most molten substances are located in the middle of the track. During the friction generation, materials from the edge zones of the track are likely extruded from the track, whereas substance at the center of the track tends to be trapped.

4.3. The crystal and steel pairs

Fig. 11 presents the surface characteristics of steel samples after rubbing with HMX and RDX sliders. This provides useful information on the friction mechanisms between steel and explosive crystals. Fig. 11(a) shows a surface track of about 30 µm in width on a roller steel sample after rubbing against an HMX slider. ESEM images do not show this particular track. In Fig. 11(b) and (c), images taken by ESEM show one track about 27.0 µm in width on the gauge steel surface after rubbing with an RDX slider. The track is composed of many amorphous particles. Because steel is much harder than explosive crystal, mass transfer from the crystal to the steel surface is responsible for such a track. The friction between crystals and their fractured particles play a vital role in the generation of frictional between explosive crystals and steel. Accordingly, the friction coefficients for crystal and steel pairs are close to those for identical crystal pairs. With the PETN slider rubbing against the steel sample, no tracks are found on the steel sample but damage is visible on the PETN sliders. Fig. 11(d) and (e) presents the damaged surface with fractured debris from the PETN slider. Friction between the PETN slider and the steel sample provides a picture of the frictional interaction between soft and hard materials. Wear on the soft material (PETN slider) may contribute more to the frictional interaction, leading to a decreased dependence of the friction coefficient on the loading force.

5. Discussions and conclusions

The coefficients of friction as a function of loading force for identical crystal pairs, dissimilar crystal pairs, and crystal sliders with steel were measured using a friction machine. For identical crystal pairs, to provide an explicit formulation of the coefficients of friction as a function of loading force, an estimate of the contact area should first be performed. In elastic regime, assuming a Hertzian contact of a spherical surface (with radius of R) indent on a flat surface, the contact area A is given by [30],

$$A = \pi \left[\frac{3}{2} \left(\frac{1-\nu^2}{E} \right) FR \right]^{\frac{2}{3}} \tag{3}$$

where E and ν are Young's modulus and Poisson ratio of the sample material, and F is the loading force. Then, the coefficient of friction in the case of two elastically deforming surfaces is given by,

$$\mu = \frac{\tau(\gamma, \dot{\gamma}, T)A}{F} = \tau(\gamma, \dot{\gamma}, T)\pi \left[\frac{3}{2} \left(\frac{1-\nu^2}{E} \right) R \right]^{2/3} F^{-1/3} \tag{4}$$

In the case of plastic contact,

$$\mu = \frac{\tau(\gamma, \dot{\gamma}, T)}{\sigma_y} \tag{5}$$

where σ_y is the yield strength. In order to obtain the explicit results, Molinar et al. [31] used a power-law- type of constitutive model, with parameters like the shear strain (γ), shear strain rate ($\dot{\gamma}$), and temperature (T),

$$\tau(\gamma, \dot{\gamma}, T) = \kappa \gamma^m \dot{\gamma}^n T^{-\upsilon} \tag{6}$$

In the case of elastic contact during friction sliding, shear stress τ changes only slightly. According to Eq. (6), we can see that the coefficients of friction (μ) generally decrease with increasing normal loading force (F). In comparison, from Eq. (7), for plastic contact, μ does not explicitly depend on F which is consistent with the measured results.

The aforementioned analyses do not apply to dissimilar crystal pairs. This may due to their different mechanical properties of sliders and the samples. The contact surfaces do not enter into the plastic regime at the same time. It is, therefore, more difficult to express the explicit dependence of friction coefficients on loading force in dissimilar crystal pairs.

Some error bars in Figs. 4–6 seem to be too wide, which may be attributed to two causes. The friction coefficient can be evaluated by,

$$\mu = \frac{(\tau \cdot A_f)}{(\sigma \cdot A)} \tag{7}$$

where A_f is the perfect adhesion area, A is the total asperity contact area, and σ is the contact stress. First, each data point was derived from repeated friction sliding at least five cycles along the same friction track. Consequently, initial cycles plough and wear the surface, changing the surface morphology. The latter cycles will thus have different values for A_f/A, and elastic contact stress σ_e from that of initial cycles. Second, at a higher loading force, contact stress (σ) roughly equals to yield stress (σ_y). However, frictional heating may not be negligible. In particular, with the appearance of molten substance, great differences in shear stress (τ) are necessary to overcome the junction between former and latter cycles.

Amuzu et al. carried out some friction experiments involving explosive single crystal on single crystal, single crystal on glass, and a thin film of explosive material between smooth rigid substrates [29]. However, additional information on the surface characteristics of the material was not provided. As such, their results did not completely agree with the data obtained in this study, especially in terms of the effects of the shapes and surface characteristics of explosive crystals. The HMX crystals had the highest friction coefficients, followed by PETN, and then by RDX. For the same crystal pairs, higher coefficients of friction were obtained at elastic stages, whereas the coefficients of friction changed little with increasing loading force when the yield point was exceeded. However, for dissimilar explosive crystals, no obvious elastic stages were observed. This may result from the non-simultaneous entry of the slider and the sample into the plastic region. Observations of the frictional sliding tracks on the sample surfaces, as well as on the sliders, measured by ESEM, indicate different possible frictional mechanisms. For the PETN slider on a PETN, the RDX slider on the $(1\,\bar{1}\,0)$ and $(1\,0\,\bar{1})$ PETN crystal planes, and the HMX slider on the $(1\,\bar{1}\,0)$ PETN plane, molten substances were observed in the tracks. These substances might act like lubricants leading to either constant or decreased friction coefficients with increasing loading force. Some orientation-dependent friction properties were also observed.

Acknowledgements

The authors would like to thank Dr. M.M. Chaudhri of the Cavendish Laboratory, University of Cambridge, the Chinese National Nature Science Foundation (Grant No. 108320[illegible] and No. 10902016), and the State Key Laboratory of Science and Technology in Beijing Institute of Technology (Project No. [illegible]03A)

References

[1] L. Avrami, R. Hutchinson, The sensitivity to impact and friction, in: H.D. Fair, R.F. Walker (Eds.), Energetic Materials: Technology of the Inorganic Azides, Plenum Press, New York, 1977, p. 144.
[2] Ch. Proust, S. Hawksworth, R. Rogers, M. Beyer, D. Lakic, D. Raveau, P. Herve, V. Pina, C. Petitfrere, X. Lefebvre, Development of a method for predicting the ignition of explosive atmospheres by mechanical friction and impacts (MECHEX), J. Loss Prevent. Proc. 20 (2007) 349–365.
[3] F.P. Bowden, A.D. Yoffe, Fast Reactions in Solids, Butterworth, London, 1958.
[4] N. Fischer, T.M. Klapötke, J. stierstorfer, New nitriminotetrazoles-synthesis, structures and characterization, Z. Anorg. Allg. Chem. 635 (2009) 271–281.
[5] M.M. Chaudhri, The initiation of fast decomposition in solid explosives by fracture, plastic flow, friction, and collapsing voids, in: Proc. 9th Symposium (International) on Detonation, Oregon, August/September, 1989, pp. 857–867.
[6] M.M. Chaudhri, Stab initiation of explosion, Nature 263 (1976) 121–122.
[7] F.P. Bowden, O.A. Gurton, Initiation of solid explosives by impact and friction: the influence of grit, Proc. R. Soc. Lond. A 198 (1949) 337–349.
[8] F.P. Bowden, D. Tabor, The Friction and Lubrication of Solids, Clarendon Press, Oxford, 1950.
[9] J.E. Field, N.K. Bourne, S.J.P. Palmer, S.M. Walley, J. Sharma, B.C. Beard, Hot-spot ignition mechanisms for explosives and propellants, Phil. Trans. Proc. R. Soc. Lond. A. 339 (1992) 269–283.
[10] G.W. Swallowe, J.E. Field, The ignition of a thin layer of explosive by impact: the effect of polymer particles, Proc. R. Soc. Lond. A. 379 (1982) 389–408.
[11] S. Hawksworth, R. Rogers, M. Beyer, Ch. Proust, Mechanical ignition hazards, in: Communication to the IMECHE Symposium, UK, 2004.
[12] S. Hawksworth, R. Rogers, Ch. Proust, M. Beyer, S. Schenck, J. Gummer, Mechanical ignition hazards in potentially explosive atmospheres—EC project MECHEX, in: Communication to the International ESMG Symposium, Nurnberg, Germany, 2004.
[13] W.H. Andersen, Role of the friction coefficient in the frictional heating ignition of explosives, Propell. Explos. 6 (1981) 17–23.
[14] M. Williams, M. Wingrave, The effect of humidity on the friction sensitiveness of RDX, Propell. Explos. Pyrot. 27 (2002) 241–243.
[15] J. Zhang, T.L. Zhang, L. Yang, J.G. Zhang, Y. Cui, X.C. Hu, Z.H. Liu, Synthesis, thermal decomposition, and properties of $[Mn(CHZ)_3]\ [C(NO_2)_3]_2$, Propell. Explos. Pyrot. 34 (2009) 24–31.
[16] D.M. Badgujar, M.B. Talawar, S.F. Harlapur, S.N. Asthana, P.P. Mahulikar, Synthesis, characterization and evaluation of 1,2-bis(2,4,6-trinitrophenyl) hydrazine: a key precursor for the synthesis of high performance energetic materials, J. Hazard. Mater. 172 (2009) 276–279.
[17] T.M. Klapötke, J. Stierstorfer, B. Weber, New energetic materials: synthesis and characterization of copper 5-nitriminotetrazolates, Inorg. Chim. Acta. 362 (2009) 2311–2320.
[18] H. Östmark, U. Bemm, H. Bergman, A. Langlet, N-guanylurea-dinitramide: a new energetic material with low sensitivity for propellants and explosives applications, Thermochim. Acta. 384 (2002) 253–259.
[19] O.H. Johansen, J.D. Kristiansen, R. Giersϕe, A. Berg, T. Halvorsen, K. smith, G.O. Nevstad, RDX and HMX with reduced sensitivity towards shock initiation—RS-RDX and RS-HMX, Propell. Explos. Pyrot. 33 (2008) 20–24.
[20] C. Rossi, D. Estève, Micropyrotechnics, a new technology for making energetic microsystems: review and prospective, Sens. Actuators A-Phys. 120 (2005) 297–310.
[21] P. Crawford, K. Rainey, P. Rightley, J.E. Hammerberg, A novel experimental technique for the study of high-speed friction under elastic loading conditions, in: M.D. Furnish, Y.M. Gupta, J.W. Forbes (Eds.), AIP Conference Proceedings on Shock Compression of Condensed Matter, Springer, New York, 2003, pp. 545–548.
[22] D.M. Hoffman, J.B. Chandler, Aspects of the tribology of the plastic bonded explosive LX-04, Propell. Explos. Pyrot. 29 (2004) 368–373.

[23] D.A. Wiegand, B. Redingius, K. Ellis, C. Leppard, Evidence for friction between crack surfaces during deformation of composite plastic bonded explosives, in: M.L. Elert, W.T. Buttler, M.D. Furnish, W.W. Anderson, W.G. Proud (Eds.), AIP Conference Proceedings on Shock Compression of Condensed Matter, Springer, New York, 2009, pp. 349–352.
[24] Q.H. Zuo, J.K. Dienes, On the stability of penny-shaped cracks with friction: the five types of brittle behavior, Int. J. Solids Struct. 42 (2005) 1309–1326.
[25] J.K. Dienes, J. Middleditch, Q.H. Zuo, J.D. Kershner, On the role of crack orientation in brittle failure, in: M.D. Furnish, Y.M. Gupta, J.W. Forbes (Eds.), AIP Conference Proceedings on Shock Compression of Condensed Matter, 2003, Springer, New York, 2004, pp. 447–450.
[26] J.K. Dienes, Q.H. Zuo, J.D. Kershner, Impact initiation of explosives and propellants via statistical crack mechanics, J. Mech. Phys. Solids 54 (2006) 1237–1275.
[27] P.D. Peterson, G.R. Avilucea, R.L. Bishop, J.A. Sanchez, Individual contributions of friction and impact on non-shock initiation of high explosives, in: M. Elert, M.D. Furnish, R. Chau, N. Holmes, J. Nguyen (Eds.), AIP Conference Proceedings on Shock Compression of Condensed Matter, Springer, New York, 2007, pp. 983–986.
[28] P.M. Dickson, G.R. Parker, L.B. Smilowitz, J.W. Zucker, B.W. Asay, Frictional heating and ignition of energetic materials, in: M.D. Furnish, M. Elert, T.P. Russell, C.T. White (Eds.), Proc. AIP Conference Proceedings on Shock Compression of Condensed Matter, Springer, New York, 2005, pp. 1057–1060.
[29] J.K.A. Amuzu, B.J. Briscoe, M.M. Chaudhri, Frictional properties of explosives, J. Phys. D: Appl. Phys. 9 (1976) 133–143.
[30] S. Thimoshenko, J.N. Goodier, Theory of Elasticity, McGraw-Hill, New York, 1951.
[31] A. Molinar, Y. Estrin, S. Mercier, Dependence of the coefficient of friction on the sliding conditions in the high velocity range, J. Tribol. ASME 121 (1999) 35–41.